Award Number: W81XWH-11-2-0021

TITLE: "Threshold-Switchable Particles (TSP) to Control Internal Hemorrhage"

PRINCIPAL INVESTIGATOR: James H. Morrissey, Ph.D.

CONTRACTING ORGANIZATION: University of Illinois, Urbana, IL 61801-3620

REPORT DATE: December 2012

TYPE OF REPORT: Annual

PREPARED FOR: U.S. Army Medical Research and Materiel Command
Fort Detrick, Maryland 21702-5012

REPORT DOCUMENTATION PAGE

Form Approved
OMB No. 0704-0188

1. REPORT DATE December 2012

2. REPORT TYPE Annual

3. DATES COVERED 23 November 2011 – 22 November 2012

4. TITLE AND SUBTITLE

"Threshold-Switchable Particles (TSP) to Control Internal Hemorrhage"

5a. CONTRACT NUMBER .

5b. GRANT NUMBER W81XWH-11-2-0021

5c. PROGRAM ELEMENT NUMBER

6. AUTHOR(S)

James H. Morrissey, Rustem Ismagilov, Ying Liu, and Galen Stucky

E-Mail:

5d. PROJECT NUMBER

5e. TASK NUMBER

5f. WORK UNIT NUMBER

7. PERFORMING ORGANIZATION NAME(S) AND ADDRESS(ES)

UNIVERSITYOF ILLINOIS

URBANA IL 61801-3620

8. PERFORMING ORGANIZATION REPORT NUMBER

9. SPONSORING / MONITORING AGENCY NAME(S) AND ADDRESS(ES)

U.S. Army Medical Research and Materiel Command
Fort Detrick, Maryland 21702-5012

10. SPONSOR/MONITOR'S ACRONYM(S)

11. SPONSOR/MONITOR'S REPORT NUMBER(S)

12. DISTRIBUTION / AVAILABILITY STATEMENT

Approved for Public Release; Distribution Unlimited

13. SUPPLEMENTARY NOTES

14. ABSTRACT

The final goal of this project is to develop smart particles to stop internal hemorrhage at local sites. Four collaborating laboratories are working together under this contract to define threshold levels of activators of blood clotting such that the candidate clotting activators will circulate in the blood at a concentration below the threshold necessary to trigger clotting, but accumulation of the activators at sites of internal injury/bleeding will cause the local concentration of clotting activators to exceed the clotting threshold and restore hemostasis. During the past year we have applied our improved methods for covalently attaching inorganic polyphosphate (a potent initiator and accelerator of blood clotting) to nanoscale solid supports including silica- and gold-based nanoparticles that have been fabricated using a variety of derivitization and passivation methods. We have conducted extensive testing of candidate procoagulant nanoparticles to quantify their ability to trigger and/or accelerate blood clotting and have made significant progress toward the goal of adjustable procoagulant activities of the particles to render them sub- or supra-threshold with regard to initiation of the clotting cascade.

15. SUBJECT TERMS

Internal hemorrhage; Bleeding; Blood clotting; Nanoparticles; Trauma

16. SECURITY CLASSIFICATION OF: a. REPORT	b. ABSTRACT	c. THIS PAGE	17. LIMITATION OF ABSTRACT	18. NUMBER OF PAGES	19a. NAME OF RESPONSIBLE PERSON
U	U	U	UU	29	USAMRMC
					19b. TELEPHONE NUMBER *(include area code)*

Table of Contents

SECOND ANNUAL REPORT: WQ81XWH-11-2-0021: "Threshold-Switchable Particles (TSP) to Control Internal Hemorrhage"

INTRODUCTION

The final goal of our research is to develop smart particles to stop internal hemorrhage at local sites. In our continuing studies toward accomplishing this goal, we are combining multiple approaches in four collaborating laboratories to define threshold levels of activators of blood clotting such that the candidate clotting activators will circulate in the blood at a concentration below the threshold necessary to trigger clotting, while accumulation of the activators at sites of internal injury/bleeding will cause their local concentration to exceed the clotting threshold and restore hemostasis. The approaches being used include the development and application of chemistries for attaching inorganic polyphosphate (polyP; a potent trigger and accelerator of blood clotting) to nanoscale solid supports, development of candidate nanoparticles with varying abilities to trigger and/or accelerate blood clotting, and defining the threshold levels under which these particles will or will not trigger blood clotting.

BODY

Comments on Administrative and Logistical Matters

Subcontracts — Four laboratories participate in this project, headed by Drs. James Morrissey (University of Illinois at Urbana-Champaign), Ying Liu (University of Illinois at Chicago), Rustem Ismagilov (originally at the University of Chicago; now at Caltech), and Galen Stucky (University of California at Santa Barbara). The primary contract was awarded to the University of Illinois, with Dr. Morrissey as the PI. The Morrissey and Liu laboratories are at University of Illinois campuses (Urbana-Champaign and Chicago), so subaward contracts were not needed and grant accounts were set up for both investigators during the first quarter. The laboratories of Drs. Ismagilov and Stucky are located at other universities, which required negotiating subcontracts to both of these sites. The subaward agreement to the University of Chicago (Ismagilov lab) was completed in February 2011, and the subaward agreement with the University of California at Santa Barbara (Stucky lab) was completed in March 2011. Dr. Ismagilov moved his laboratory to Caltech in October 2011, and a new subaward contract to Caltech was finalized at the end of May 2012 in order for Dr. Ismagilov to continue his studies funded in this project.

Human Anatomical Substances use approval (Milestone #2) — Some of the studies to be conducted in Dr. Ismagilov's lab employ blood samples from human volunteer blood donors, which requires regulatory approval. Dr. Ismagilov obtained IRB approval from Caltech for these studies (RI-334, approved on December 5, 2011) and this was communicated on Thursday, December 8, 2011 to Ms. Brigit Ciccarello (Regulatory Compliance Specialist, Telemedicine & Advanced Technology Research Center, U.S. Army Medical Research and Materiel Command, Fort Detrick, Maryland), who submitted the necessary documents to obtain approval from the Office of Research Protections. Dr. Ismagilov was notified on March 20, 2012 that the protocol has been approved by the Office of Research Protections. IRB protocol 12502A at the University of Chicago, which conferred approval on the Ismagilov lab's work on the project prior to their move to Caltech, was closed on March 2, 2012. Thus, the subaward agreement has been implemented at Caltech and the necessary human subjects regulatory approvals have been obtained at Caltech.

Scientific Progress

BACKGROUND

Inorganic polyphosphate (polyP) is a linear, unbranched polymer composed of orthophosphate monomers. Extremely conserved and ubiquitous across a diverse range of organisms, its physiological function in humans and other complex eukaryotes has only recently been broadly elucidated [1]. PolyP is secreted from the dense granules of activated platelets and acts at various stages of the coagulation cascade depending on its polymer length [2].

Long-chain polyP (generally greater than 500 phosphate monomers long) serve as potent contact surfaces for initiation of the intrinsic pathway, while shorter polyP polymers of 60-100 phosphate units catalyze the conversion of the zymogen Factor V to its active form and slow the breakdown of fibrin clots [2, 3]. With its role now clearly established as a critical hemostatic agent within the body, polyP could potentially serve as a useful and safe procoagulant compound to address multiple bleeding disorders including internal hemorrhage.

When intravenously administered, nanoparticle therapies have been devised to target activated platelets with some success, but the goal of functionally delivering a procoagulant therapy to treat internal hemorrhage in practice has yet to be fully realized [4]. We are developing novel approaches for the targeted delivery of nanoparticles functionalized with controlled amounts of polyP. These tunable particles will then be able to selectively target sites of injury in response to appropriate stimuli such as a drop in temperature without the induction of clotting anywhere else in the body, a property that aqueous polyP unfortunately does not possess. Therefore, the goal of this study is to understand the process of particle-induced blood clotting, which could eventually lead to optimally engineered particles for coagulation.

A. Studies in the Morrissey lab (toward Task 3, Milestone 4)

The Morrissey lab has worked to develop methods for reproducibly size-fractionating polyP in larger quantities than have been previously available, in ways that can be scaled to yield even larger quantities of fractionated polyP. In early studies, we employed preparative polyacrylamide gel electrophoresis to isolate carefully size-fractionated preparations of polyP, starting with various highly heterogeneous polyP preparations. While this method is robust and reproducible, it suffers from the drawback that only milligram quantities of size-fractionated polyP can be prepared per batch. Nanoparticle preparations underway in the Stucky and Liu labs require gram quantities of size-fractionated polyP. We therefore worked to develop alternative, scalable means for preparing fractionated polyPs of the desired ranges of polymer lengths, and have been successful.

We found that we can use a very high MW polyP preparation (marketed as "insoluble sodium phosphate glass") as the starting material for preparing polyP fractions of the desired polymer lengths. Very high MW polyP is largely insoluble in water, as it consists mostly of polymers that are thousands of phosphate units long. We investigated a number of methods for solubilizing high MW polyP and found that suspending the material in nonbuffered 100^{o}C 0.25 M LiCl solution with constant stirring resulted in the majority of the polyP going into solution. Furthermore, we observed a time-dependent shortening of the average polymer length of the polyPs during heating (Figure A). Further investigations revealed that the slightly acidic pH of the polyP solutions was resulting in a mild acid hydrolysis of the polymers. Curiously, the speed of hydrolysis appeared to increase with time, which we found was the result of the gradual acidification of the solution as the polyP polymers were being hydrolyzed. The fact that two protons should be released following the cleavage of each phosphoanhydride bond in polyP is doubtless the basis for this. The gradual acidification of the polyP solution therefore gradually accelerates the rate of polyP hydrolysis, which made the reactions difficult to control precisely.

Figure A - PAGE of material acquired during time course of hydrolysis with unbuffered LiCl.

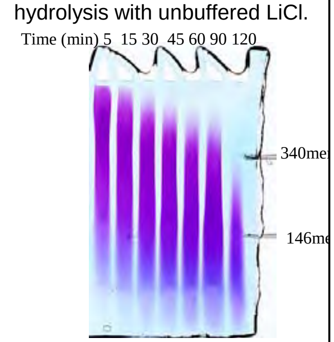

Hydrolysis of the phosphoanhydride bonds in polyP can also be catalyzed under basic conditions, and we reasoned that the gradual acidification of the solution during polyP hydrolysis would serve to gradually slow the rate of hydrolysis, in contrast to acid hydrolysis whose rate increases with time. We therefore tested adding varying amounts of LiOH to the LiCl solutions in which polyP was stirred at 100ºC. We observed a gradual, time-dependent shortening of polyP chains as a function of the starting LiOH concentration, which was accompanied by the "insoluble" polyP polymers becoming water-soluble (Figure B). Furthermore, we found that the rate of base-catalyzed polyP degradation was far easier to control than the rate of acid-catalyzed degradation. Accordingly, we have now identified conditions in which high MW polyP is suspended, with stirring, in a combination of LiCl and LiOH at 100ºC until the desired mean polymer lengths have been obtained and essentially 100% of the material is solubilized. This method is robust and reproducible, and unlike the use of preparative electrophoresis, is easily scalable to gram quantities of polyP and higher.

Figure B - PAGE of material acquired during time course of hydrolysis with alkaline LiCl.

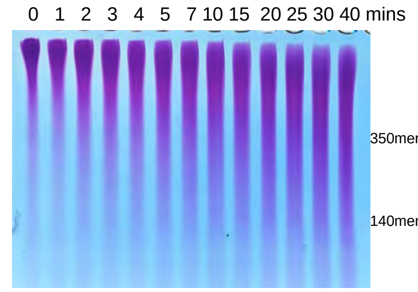

Figure C - PAGE of size fractionated high yield polyP

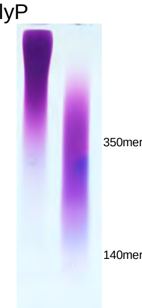

We have found that, although the conditions for solubilizing and partially hydrolyzing polyP with LiOH/LiCl can be easily adjusted to yield the desired mean polymer lengths, the method nevertheless results in polyP preparations of somewhat heterogeneous sizes. We therefore sought a scalable method to further size-fractionate polyP after limited base hydrolysis. Initially, we had employed differential precipitation of polyP using varying combinations of acetone and salt concentrations (with the latter also varying between NaCl, KCl and LiCl, which differentially affect polyP solubility). However, scaling up acetone precipitations has drawbacks, including the very high volatility and flammability of acetone. We therefore examined a variety of precipitants and found that combinations of varying concentrations of isopropanol and NaCl allowed us to obtain relatively narrow size fractions of polyP, starting with high MW polyP that had previously been solubilized and partially hydrolyzed using the LiOH/LiCl procedure outlined above (see Figure C for an example). We have now identified conditions in which we can obtain essentially any desired size ranges of polyP, from ~40 to ~1500 phosphate units long, in gram quantities and above. The Morrissey lab has provided gram quantities of these size-fractionated polyP preparations to the Stucky and Liu labs for use in nanoparticle formulation.

B. Studies in the Ismagilov lab

The Ismagilov lab's move from the University of Chicago to the California Institute of Technology delayed progress during the second year, since the subaward agreement with Caltech was not completed until the end of May 2012. Now that the subaward agreement is in place with Caltech, the Ismagilov lab is working to hire personnel so that progress toward Tasks 1-4 can proceed in the coming contract period.

C. Studies from the Liu lab (in collaboration with the Morrissey lab): Citrate gold nanoparticle synthesis (toward Task 3, Milestone 4)

Gold nanoparticles with an average diameter of 10nm, 15nm, and 50nm were synthesized in the Liu lab by using the Turkevich Method [5]. The average size and size distribution of the gold nanoparticles were confirmed by dynamic light scattering (DLS) and UV-vis absorbance (Table 1 and Figure 1).

Table 1. Comparison of the lab-made 10nm, 15nm, 50nm gold nanoparticles and the commercial samples with their UV-vis peak, DLS-measured particles size and polydispersity.

	Mole ratio (Cg : Cc)	Gold Concentration	Reaction Temperature	UV Peak	Size	Polydispersity
Reaction A	1:4	0.4mM	95^{o}C	520nm	13.6nm	0.175
			60^{o}C	522nm	14.7nm	0.25
Reaction B	1:3	0.4mM	95^{o}C	522nm	17.2nm	0.178
			60^{o}C	522nm	18.3nm	0.227
Reaction C	1:1	0.4mM	95^{o}C	533nm	35.7nm	0.196
			60^{o}C	534nm	37.9nm	0.256
Commercial_10		0.29mM		519nm	11.3nm	0.24
Commercial_15		0.24mM		521nm	15.6nm	0.19
Commercial 50		2.89mM		532nm	42.1nm	0.11

Figure 1. Size distribution of gold nanoparticles measured by DLS. Molar ratio of citrate to gold was (A) 4:1 (B) 3:1 and (C) 1:1.

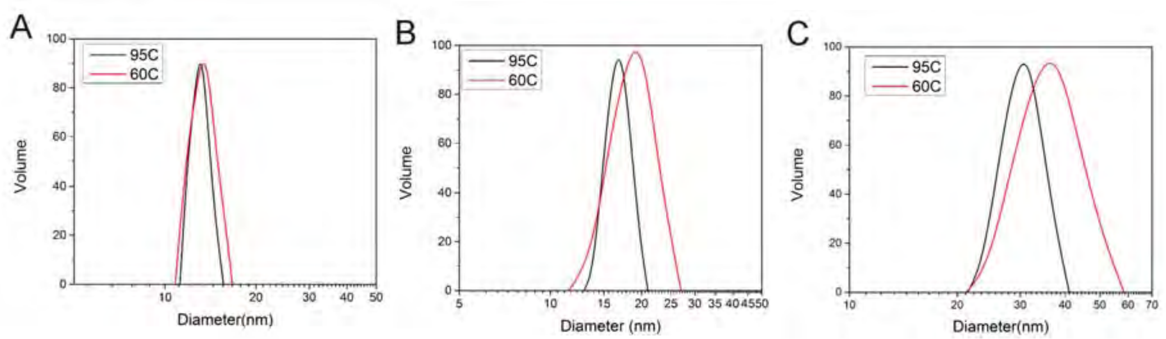

PolyP-gold nanoparticle conjugates

Attachment of polyP to gold nanoparticles was achieved by two-stage reactions. (1) PolyP was allowed to react with cystamine; (2) PolyP-cystamine conjugates were then reacted with gold particles via displacement of the citrate groups (Figure 2).

Figure 2. The process of synthesizing gold nanoparticles conjugated with polyP. (A) PolyP is conjugated to cystamine. (B) PolyP-cystamine is attached to the surface of gold nanoparticles.

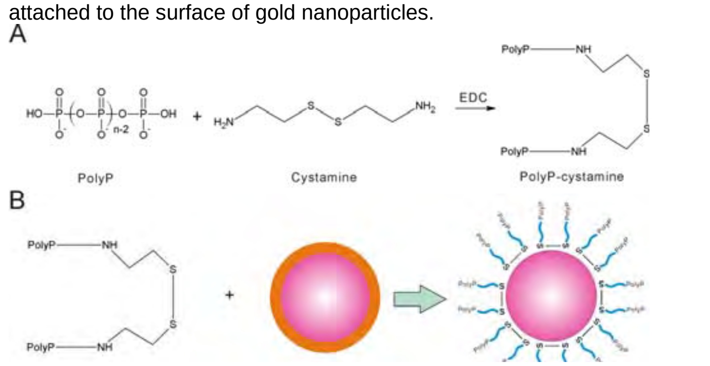

The reaction of polyP with primary amine-containing compounds was established by the Morrissey group. The primary amine-containing compounds like polyethylenimine, amine-PEG$_2$-biotyn, and spermidine were used to study the covalent attachment of primary amine groups with the terminal phosphates of polyP via EDAC-meditated reaction [6]. We utilized this method for the coupling of polyP with cystamine – a disulfide molecule, containing two primary amine groups. The disulfide moiety in cystamine then allowed for the attachment to gold. Various conditions (including temperature, reaction time, pH, and buffer solutions) were tested in order to optimize the reaction efficiency and yield.

Conjugation of polyP to gold nanoparticles was investigated in the Liu lab to verify three hypotheses: (1) blood clotting kinetics and mechanism would be affected by the size and surface properties of the particles and a threshold condition may be defined; (2) the choice of the biocompatible core material would not change the blood clotting kinetics or mechanism; and (3) when conjugated to the nanoparticles, number density of polyP (aggregation number) will affect clotting kinetics. (These address milestones 3 and 4).

The effects of polyP-gold nanoparticles (with different sizes and polyP aggregation numbers) on blood clotting kinetics were tested. The following control groups were selected to compare with polyP-gold nanoparticle conjugates: (1) free polyP with the same molecular weight at the same concentrations; (2) citrate gold nanoparticles without polyP; and (3) PEGylated gold nanoparticles. Various aggregation numbers of polyP on gold nanoparticles were achieved by adding PEG thiol to compete with polyP-cystamine for ligand replacement.

PolyP-cystamine conjugation reaction

Various conditions (including temperature, reaction time, pH, and buffer solutions) were tested in order to optimize the coupling reaction of polyP with cystamine. For the optimal conditions, polyP was allowed to react with cystamine at room temperature for 48 to 72hrs. The optimal pH for the reaction was around 8. Higher temperature (37 °C) did not help, resulting in similar yields as at room temperature. A fluorescamine assay was used to test the amount of the unreacted primary amines on cystamine, which indicated the conjugation efficiency. The yield of the reaction at optimized conditions was approximately 90% as seen in (**Table 2**).

Table 2. Conjugation efficiency of polyP and cystamine at various pH conditions.

Buffer	pH of reaction	Efficiency (24h)	Efficiency (48h)	Efficiency (72h)
MOPS (100 mM)	7.1	61.5%	65.0%	71.1%
MOPS(100 mM)	7.6	72.7%	74.3%	78.7%
MOPS(100 mM)	8.1	79.6%	87.3%	88.1%
MOPS(100 mM)	8.5	83.5%	87.3%	88.6%
MES(100 mM)	7.8	81.4%	89.5%	-

The hydrolysis study of the P-N bond was carried out to test the stability of the polyP-cystamine ligand. After 72 hours of reaction, the fluorescamine assay was performed to detect the concentration of the unreacted cystamine. An increase of free cystamine concentration after the pH adjustment of reactions indicated the hydrolysis of the P-N bond. The samples were tested for two weeks and quantified by the fluorescamine assay. The P-N bond hydrolyzed in acidic conditions at pH 6.02. It was stable above pH 7 as seen in **Table 3** below.

These results were in good agreement with other literature data on P-N bond hydrolysis.[7-11]

Table 3. Free cystamine concentration (μM) before and after pH adjustment.

pH	Primary amine concentration (μM)				
	Before pH adjustment	After 1 day	After 5 days	After 8 days	After 13 days
6.02	16.4	30.0	26.4	27.6	37.18
7.07	16.4	18.6	14.5	12.9	13.72
9.05	16.4	17.1	14.8	14.2	15.31
10.01	16.4	17.2	14.8	12.7	14.73

Reaction of polyP-cystamine with gold nanoparticles

The polyP-cystamine conjugate was allowed to react with gold nanoparticles of various sizes (10nm, 15nm, 50nm) by displacing the citrate group. After 24hrs of reaction the salt addition was initiated to increase the coverage of the surface of the gold nanoparticle with polyP. The slow increase in the salt concentration in the reaction over a period of four days (0.1M NaCl final concentration) allowed for the already attached polyP to extend, creating more space for the unreacted ligands to access the gold surface and thus resulting in an increase in the aggregation number. This method of increasing the ionic strength of solution to 0.1 M salt concentration was previously reported by the Mirkin group at Northwestern University [12]. We adopted this technique and optimized it for our specific reaction conditions.

The purification process of gold nanoparticles involved the removal of excess, free floating polyP left in the solution. Centrifugation was used to obtain the optimal conditions for the removal of ~99% free floating polyP and for the recovery of most of the gold particles (~90%) without causing any aggregation. Depending on the size of the gold nanoparticles, the following optimal conditions were found (**Table 4**). The pelleting time, *t*, was calculated using the flowing **Equation 1** [13, 14]:

Table 4. Size-dependent centrifugation conditions.

Au NPs size	RPM	G force	Time to pellet	Centrifuge repeat
10 nm	10000	8176	60 min	3x
15 nm	10000	8176	30 min	2x
50 nm	8000	5223	10 min	3x

$$t = \frac{k}{S}$$

where *k* is the pelleting efficiency of the rotor and *S* is the sedimentation coefficient. The pelleting efficiency (*k*) was calculated by using **Equation 2** below [13, 14]:

$$k = \frac{2.5x10^{11} \ln\left(\frac{r_{max}}{r_{min}}\right)}{RPM^2}$$

r_{max} and r_{min} are the maximum and minimum radii of the centrifuge respectively, and RPM is the speed in revolutions per minute. The r_{max} and r_{min} values can be measured as shown in the **Figure 3** based on the type of centrifuge used [15].

The sedimentation coefficient, *S*, can be calculated by using **Equation 3** [13, 14]:

$$S = \frac{2(\rho_s - \rho_l)}{9\eta}\left(\frac{d}{2}\right)^2$$

where ρ_s and ρ_l are the densities of gold nanoparticles and water, respectively, η is the viscosity of water, and *d* is the diameter of gold nanoparticles.

After each centrifugation, the supernatant was removed and the pellets were re-suspended in a buffer of pH 7.4 to ensure the stability of the polyP-cystamine ligand. As the hydrolysis study showed, the pH of the samples played a tremendous role in P-N bond hydrolysis. Therefore, it was necessary to resuspend the particles with a buffer at a pH higher than 7.

Figure 3. Determination of the minimum and maximum radius based on the geometry of a centrifuge.

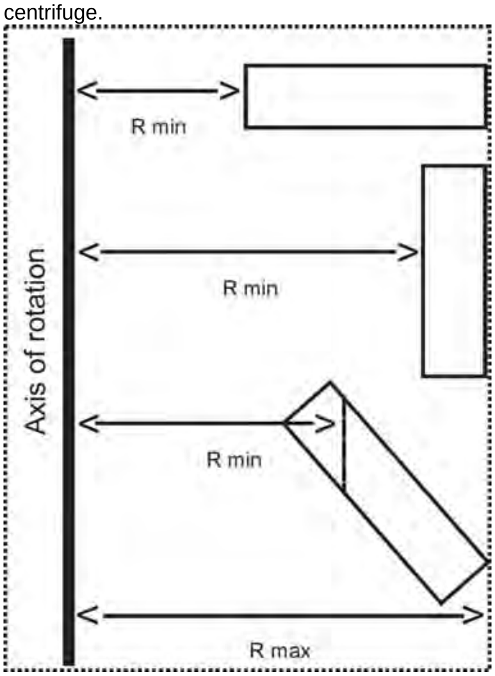

Dynamic light scattering and UV-vis spectroscopy were used to characterize the size and size distribution of the particles. After purification/separation using centrifugation, concentrations of polyP were measured using malachite green assay and concentrations of gold nanoparticles were obtained by UV-vis. Then aggregation numbers of polyP on the surface of gold nanoparticles were calculated based on the above measurements. The following polyP-gold nanoparticles (**Table 5-7**) were synthesized and characterized.

Table 5. Synthesized polyP45-gold nanoparticles.

Sample	PolyP size (# of repeating units)	MonoP Conc. (μM)	Gold Particle Conc. (nM)	Aggregation #	UV-vis peak for bulk gold	Peak after centrifuging
P45_10nm_1	45	80.00	104.7	16.98	519	523
P45_10nm_2	45	80.00	90.34	19.68	519	524
P45_15nm_1	45	80.00	29.29	60.70	521	523
P45_15nm_2	45	80.00	37.33	47.62	521	523
P45_50nm_1	45	80.00	3.74	475.34	533	533
P45_50nm_2	45	80.00	2.03	875.75	533	533

Table 6. Synthesized polyP70-gold nanoparticles.

Sample	PolyP size	MonoP Conc. (μM)	Gold Particle Conc. (nM)	Aggregation #	UV-vis peak for bulk gold	Peak after centrifuging
P70_10nm_1	70	75.00	31.98	33.50	519	524
P70_10nm_2	70	75.00	153.50	6.98	519	528
P70_15nm_1	70	75.00	16.14	66.38	521	522
P70_15nm_2	70	75.00	32.05	33.43	521	522
P70_50nm_1	70	75.00	2.068	518.09	532	533
P70_50nm_2	70	75.00	2.010	533.05	532	533

Table 7. Synthesized polyP-PEG (3:1)-gold nanoparticles.

Sample	PolyP	MonoP Conc. (μM)	Gold Particle Conc. (nM)	Aggregation #	UV-vis peak for bulk gold	Peak after centrifuging
P70_Peg_10nm_1	70	75.00	76.00	14.1	519	525
P70_Peg_15nm_1	70	75.00	34.69	30.88	521	521
P70_Peg_50nm_1	70	75.00	3.83	279.7	532	533
P45_Peg_10nm_2	45	75.00	73.14	22.79	519	523
P45_Peg_15nm_2	45	75.0	35.50	46.95	521	526

Effects of polyP-gold nanoparticle on blood coagulation kinetics – measured by coagulometry.

The samples presented in the section above were sent to the Morrissey group (UIUC) for clotting tests using coagulometry. The experiments performed by the Morrissey group focused on contact pathway activation. The activation of the contact pathway by polyP-gold nanoparticles is expressed in terms of equivalent long-chain polyP concentrations (**Figure 4** and **5**). Long-chain polyP, which is a heterogeneous mixture of polymers greater than 500 repeating units, can induce the intrinsic contact pathway of blood coagulation. The initial results indicated that the polyP45-gold nanoparticle samples had superior procoagulant activity when compared with free-floating polyP45 of the same concentration in solution (**Figure 4**). For each particle diameter of the polyP45-gold nanoparticle samples that were synthesized, there was a direct correlation between aggregation number and increased procoagulant activity. However, this trend does not appear to hold when comparing across particle sizes. An increased activity of some 10 and 15 nm samples when compared to 50nm may be due to agglomeration of smaller size gold nanoparticles as indicated by the UV-vis peak shift after purification. A conclusion still remains unclear at this point because there are two phenomena occurring that must be considered: the surface density of the procoagulant ligand polyP and the total surface area of the gold. Moreover, more measurements must be taken in order to establish statistical significance of the results. The citrate gold nanoparticles also acted as contact pathway initiators due to their negative surface charges, although not to as great as an extent as the polyP-gold nanoparticle conjugates.

Figure 4. Cumulative clotting activity for 10nm, 15nm, and 50nm polyP45-gold nanoparticles (Please refer to **Table 5** for sample information).

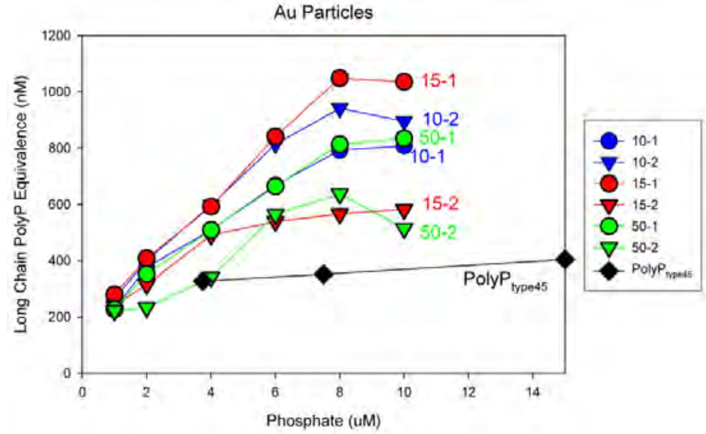

Figure 5. Cumulative clotting activity for 10nm, 15nm, and 50nm polyP70-gold nanoparticles (Please refer to **Table 6** and **7** for sample information).

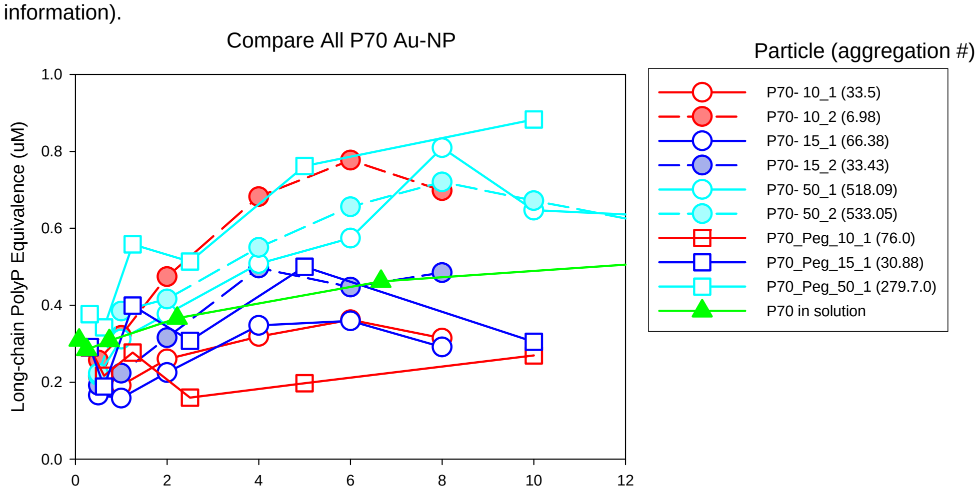

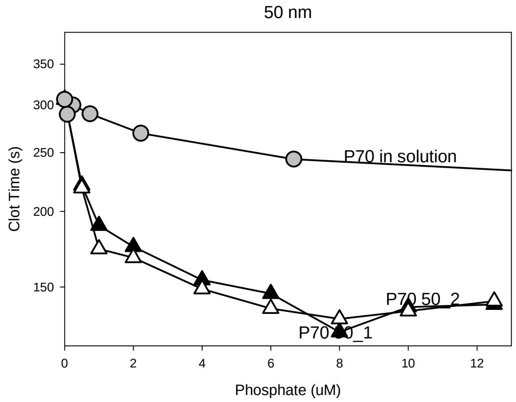

Figure 6. Contact pathway activation of polyP70-50nm gold nanoparticles (please refer to **Table 6** for sample information) at a constant gold particle concentration.

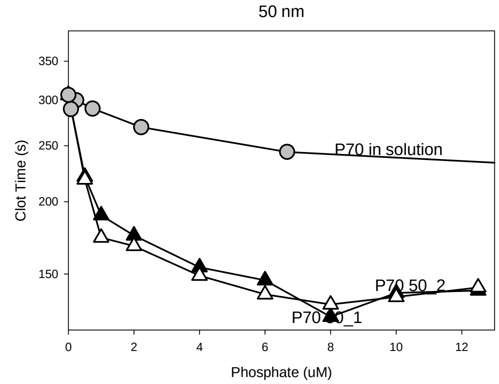

Figure 7. Contact pathway activation data for polyP70-50nm gold nanoparticles (please refer to **Table 6** for sample information) at constant phosphate concentration.

The initial contact pathway activation coagulometry experiments for polyP70-gold nanoparticles showed only an increased activity of 50nm polyP70-gold samples when compared to free floating polyP70 in solution. There was no significant difference between the 10 and 15nmpolyP70-gold nanoparticles and corresponding aqueous polyP70 (**Figure 5**). The superior activity of the 50nm polyP70-gold nanoparticle can be seen in **Figures 6-8**. The fully PEGylated 50nm gold nanoparticle as a negative control did not show any procoagulant activity **(Figure 8**). The partially PEGylated 50 nm polyP70-gold nanoparticle (with less polyP conjugated to gold nanoparticles) showed reduced procoagulant activity as expected, which was still more active than free-floating polyP70 at the same concentration. More experiments are needed in order to establish statistically significant trends such as the threshold size conditions and critical average surface coverage of polyP.

Despite the fact that no conclusions can be drawn on critical parameters for clotting induction including particle diameter and aggregation number, the results appear to be highly promising given that the polyP-functionalized gold particles appear to be much more robustly procoagulant than aqueous polyP of the same polymer length. More important, 50nm may be the criticial size for the particles to induce blood coagulation. Therefore, we can use controlled aggregation to switch the size of the particles by the local physiological conditions at the trauma sites.

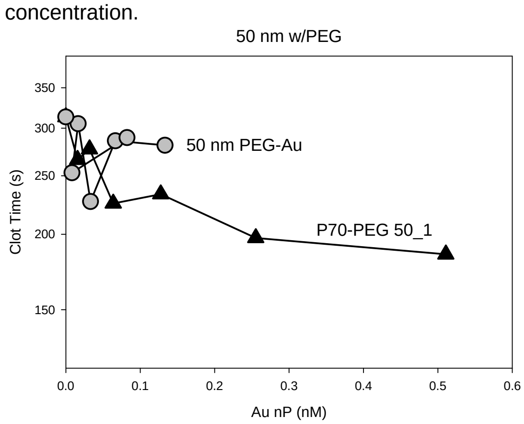

Figure 8. Contact pathway activation data for polyP70-Peg (3:1)-50nm gold nanoparticles (please refer to **Table 7** for sample information) at constant gold nanoparticle concentration.

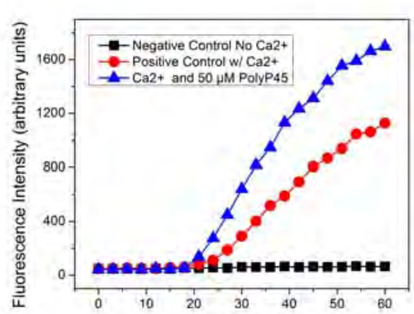

Figure 9. Preliminary fluorescent measurements for induction of the contact pathway with aqueous polyP45 using a fluorogenic thrombin substrate.

Blood coagulation kinetics – measured by microplate-based florescent assays

Activation of the intrinsic pathway of blood coagulation was assessed by using a fluorogenic thrombin substrate [16]. A negative control containing no Ca^{2+}, and a positive control containing no polyP were also run to ensure the validity of the experiment. To find the clotting time, the data were fitted to a sigmoidal function. The rate of thrombin substrate cleavage was found by taking the time derivative of the fluorescence intensity of the fitted curve, and the clotting time was defined in the relevant samples to be one-half the maximum rate of substrate cleavage. Clotting kinetics was first measured using free polyP45. Clotting induction occurs only in the presence of calcium cations (**Figure 9**), which is consistent with the results previously reported by Morrissey group [1-3]. More quantitative measurements on clotting kinetics through contact, tissue factor, and FV pathways using polyP45, long chain polyp, citrate gold nanoparticles, PEGylated gold nanoparticles, and polyP-gold nanoparticles will be contacted in near future.

Controlled particle aggregation by using thermosensitive polymers

Based on our previous results, we hypothesize that controlled aggregation of smaller nanoparticles (~15nm) into bigger ones (>50nm) may trigger blood coagulation rapidly via contact pathway initiation as well as FV at the site of vessel or organ damage but not elsewhere. Our first attempt is to utilize the body temperature drop at the local trauma site due to the lack of blood and oxygen.[17] In this study, we have conjugated poly(acrylic acid) (PAAc) and polyacrylamide (PAAm) on gold nanoparticles through disulfide bonds. PAAc and PAAm are thermosensitive polymers with an upper critical solution temperature (UCST) around 33-35^{o}C [18]. When the temperature is below the UCST, PAAc and PAAm form inter-molecular hydrogen bonding, which increases the hydrophobicity of the polymers and results in aggregation of the particles and phase separation (Figure 10A). The process is reversible. When the temperature is above the UCST, the hydrogen bonding disassembles and the phase separation disappears.

Reversible hydrogen bonding

The assembly and disassembly of inter-molecular hydrogen bonding between PAAc and PAAm were observed (**Figure 10**). A mixture of 10 wt% PAAc and 10 wt% PAAm was prepared at room temperature (~ 20^{o}C), which is below the UCST. Hydrogen bonding formed immediately and resulted in turbidity of the solution, which indicates phase separation between the polymers and water (**Figure 10 B**). The sample was then heated up to 40^{o}C in a water bath. The solution turned clear, which indicated the disassembly of hydrogen bonding (**Figure 10 C**). The sample became turbid again when it was cooled back to room temperature, which indicated the reformation of hydrogen bonding and the reversibility of the process (**Figure 10 D**).

Figure 10. The assembly and disassembly of inter-molecular hydrogen bonding between PAAc and PAAm. (A) Schematic representation. (B) PAAc and PAAm aqueous solutions were mixed thoroughly at 20 ^{o}C. (C) The mixture was heated to 40 ^{o}C. (D) The solution was cooled back to 20 ^{o}C.

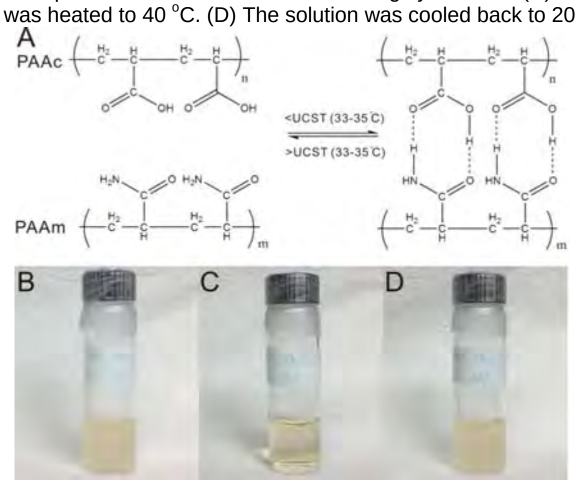

Conjugation reaction and particle characterization

Three steps are involved in synthesizing and characterizing the nanoparticles conjugated with the thermosensitive polymers, as shown in **Figure 11**. (1) PAAc and PAAm are conjugated to cystamine and 3,3'-dithiodipropionic acid (DDA) respectively which contain disulfide bonds. (2) PAAc-cystamine or PAAm-DDA is attached to the surface of gold particles through the disulfide bond. (3)The particles

are separated from the unreacted molecules by using centrifugation and characterized by using dynamic light scattering (DLS) and UV-vis spectroscopy.

Figure 11. The process of synthesizing gold nanoparticles conjugated with the thermosensitive polymers. (A) PAAc or PAAm is conjugated to cystamine or DDA. (B)PAAc-cystamine or PAAm-DDA is attached to the surface of gold nanoparticles.

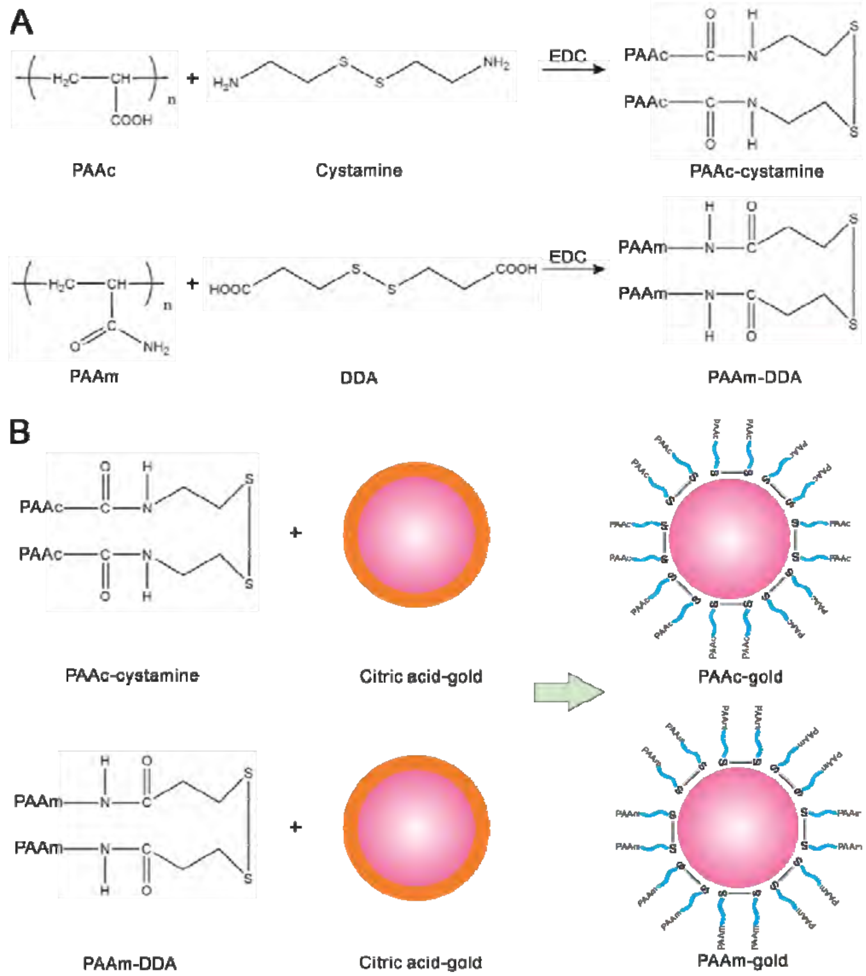

PAAc was conjugated to cystamine by using the zero-length cross-linking reagent, EDAC (1-ethyl-3-[3-(dimethylamino)propyl]carbodiimide). Different pH conditions were used to test the conjugation efficiency between PAAc and cystamine. An excess amount of PAAc was used to ensure the complete reaction of cystamine. The fluorescamine assay was utilized to test the amount of the unreacted primary amines on cystamine, which indicated the conjugation efficiency. The results were shown in **Table 8**. The reactions were very efficient at neutral and slightly basic conditions. Conjugation efficiencies above 95% have been consistently achieved for all the samples. Similar reaction conditions have been used for the reaction of PAAm with DDA.

Table 8. Conjugation efficiency of PAAc-cystamine at various pH conditions.

	pH	Efficiency (24h)	Efficiency (48h)
MES_pH4	7.2	96.1%	96.6%
MES_pH6	8.0	97.7%	95.5%
MES_pH8	9.1	96.5%	97.8%

PAAc-gold and PAAm-gold conjugation

Disulfide bonds on PAAc-cystamine and PAAm-DDA were used to replace the citrate on the surface of the gold nanoparticles through ligand exchange. PAAc-cystamine or PAAm-DDA was mixed with citrate gold nanoparticles in DI water for 24 hours. After that, 10 µL of 5M NaCl was added for four consecutive days to increase the ionic strength of the solution so that more ligands could access the gold surface. Centrifugation was used to remove unreacted polymers and reagents in the suspensions. UV-visible spectroscopy and DLS were used to confirm the sizes of PAAc-gold and PAAm-gold conjugations. The shift of the absorbance peak would indicate the aggregation of the gold nanoparticles.[19, 20]

Various conditions were tested to generate stable PAAc-gold conjugation, as shown in **Table 9**. C-N linkage shows good stability in a broad pH range from pH4 to pH9.[21] The initial ligand replacement was tested with and without buffers.

Table 9. Stability of gold nanoparticles conjugated with PAAc.

Sample ID	Gold particle size (nm)	PAAc-cystamine (0.1mM)	polyP-cystamine (0.1mM)	Buffer	UV (AS)	UV (AP)	Stability
PAAc_10nm_polyP(13)	10	7.5 µL	22.5 µL	MES (0.5 M) 120 µL	519.5	522	Yes
PAAc_10nm_polyP(11)	10	15 µL	15µL	MES (0.5 M) 120 µL	520	522	Yes
PAAc_10nm_30_MES	10	30 µL	-	MES (0.5 M) 120 µL	527	536	No
PAAc_10nm_30_BA	10	30 µL	-	BA (0.25 M) 30 µL	608	-	No
PAAc_10nm_20_BA	10	20 µL	-	BA (0.25 M) 30 µL	617.5	-	No
PAAc_10nm_30	10	30 µL	-	-	535.5	-	No
PAAc_10nm_20	10	20 µL	-	-	533	-	No
PAAc_10nm_15	10	15 µL	-	-	534.5	-	No
PAAc_15nm_15	15	15 µL	-	-	522	523	Yes

Abbreviations used in the table: AS – after salt addition and AP – after purification.

Conjugation of PAAm-DDA with gold nanoparticles to form PAAm-gold was characterized and summarized in **Table 10**.

Table 10. Stability of gold nanoparticles conjugated with PAAm.

Sample ID	Gold particle size (nm)	PAAm-DDA (0.1mM)	polyP-cystamine (0.1mM)	Buffer	UV (AS)	UV (AP)	Stability
PAAm_10nm_polyP(13)	10	7.5 µL	22.5 µL	MES (0.5 M) 120 µL	520.5	521	Yes
PAAm_10nm_polyP(11)	10	15 µL	15 µL	MES (0.5 M) 120 µL	518.5	521.5	Yes
PAAm_10nm_30_MES	10	30 µL	-	MES (0.5 M) 120 µL	527	526.5	No
PAAm_10nm_30_BA	10	30 µL	-	BA (0.25 M) 30 µL	521	524	Yes
PAAm_10nm_20_BA	10	20 µL	-	BA (0.25 M) 30 µL	519.5	521	Yes
PAAm_15nm_15	15	15 µL	-	-	530	-	No
PAAm_15nm_15_BA	15	15 L	-	BA (0.25 M) 30 L	533	-	No
PAAm_15nm_7.5_BA	15	7.5 L	-	BA (0.25 M) 30 L	525.5	525.5	Yes

Reversible particle aggregation upon temperature change

PAAc_10nm_polyP(13) and PAAm_10nm_polyP(13) were mixed at a 1:1 volume ratio. DLS and UV-visible absorbance were used to test the size of gold nanoparticles at different temperatures. The absorbance peaks of PAAc_10nm_polyP(13) and PAAm_10nm_polyP(13) were 523.5 and 522 respectively. After mixing PAAc_10nm_polyP(13) and PAAm_10nm_polyP(13) at a 1:1 ratio at 20^{o}C, the absorbance peak was 524 nm, which showed no significant increase. The aggregation of PAAc_10nm_polyP(13) and PAAm_10nm_polyP(13), if any, was caused by the formation of inter-molecular hydrogen bonding between PAAc and PAAm, which may not induce any significant peak shift since the hard core of the particles may be still sufficiently separated.

DLS was also used to test the size distribution of gold nanoparticles at different temperatures. The size of PAAc_10nm_polyP(13)and PAAm_10nm_polyP(13) peaked at 9 nm consistently at 25 °C and 37 °C.

The size and size distribution of the mixture of PAAc_10nm_polyP(13) and PAAm_10nm_polyP(13) at 25 °C, 33 °C and 37 °C are shown in **Figure 12**. Aggregation was observed at 25 °C and 33 °C. The size of PAAcm_10nm_polyP(13) at 25 °C and 33 °C was 15.2 nm and 14 nm respectively, while the original size of the gold nanoparticles by DLS was about 9 nm. When the temperature was increased to 37 °C, which is above the UCST of PAAc and PAAm, the hydrogen bonding disassembled and the size of the gold nanoparticles reduced back to about 9 nm.

Figure 12. Size distribution of the nanoparticles after mixing PAAc_10nm_polyP(13) with PAAm_10nm_polyP(13) at a 1:1 ratio at 25 °C, 33 °Cand 37 °C.

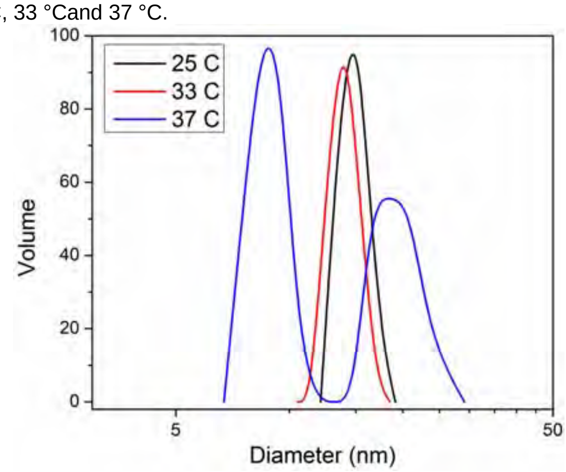

A Mixture of PAAc_10nm_polyP(11) and PAAm_10nm_polyP(11) at a 1:1 ratio also showed similar results of particle aggregation (**Figure 13**). At 25 °C, average size measured by DLS is 17.5 nm. When the temperature was increased to 37 °C, a small peak at 8 nm appeared which indicates the disassembly of the inter-molecular hydrogen bonding between PAAc and PAAm.

PAAc_10nm_polyP(11) or PAAm_10nm_polyP(11) has more PAAc or PAAm and less polyP on the surface of the gold nanoparticles as compared to PAAc_10nm_polyP(13) or PAAm_10nm_polyP(13). Thus it is relatively more difficult to disassemble all the hydrogen bonding and resuspend the nanoparticles back to their original size.

In order to generate bigger aggregation, PAAc or PAAm was conjugated to the surface of gold nanoparticles alone without polyP. However, when mixing PAAc_15nm_15 and PAAm_10nm_20_BA at a 1:1 ratio, aggregation was not found.

Figure 13. Size distribution of the nanoparticles after mixing PAAc_10nm_polyP(11) with PAAm_10nm_polyP(11) at a 1:1 ratio at 25 °Cand 37 °C. In order to generate bigger aggregation, PAAc or PAAm was conjugated to the surface of gold nanoparticles alone without polyP. However, when mixing PAAc_15nm_15 and PAAm_10nm_20_BA at a 1:1 ratio, aggregation was not found.

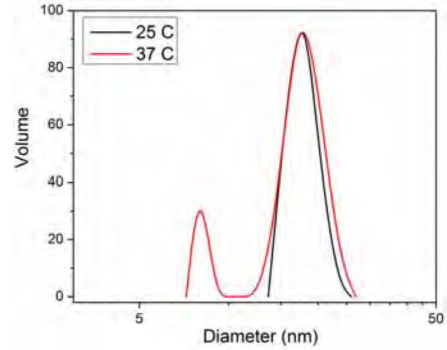

Future work in the Liu and Morrissey labs

- PolyP with polymer lengths greater than 200 units, as well as narrower polymer length distributions, will be conjugated to gold nanoparticles of various diameters.
- Coagulometry data (Morrissey Lab, UIUC) will be corroborated by the microplate-based fluorescent clotting time assay in the Liu Lab (UIC).
- After acquiring enough *in vitro* data (i.e. multiple runs to establish statistical significance) on clotting kinetics, conclusions will be drawn on threshold particle diameter and average surface density (aggregation number) of polyP.
- In addition to exploring the procoagulant activity of the particles as initiators of the contact pathway, greater focus will be also placed on induction of the extrinsic pathway of the coagulation cascade.
- Temperature-switchable aggregation larger than 50nm will be generated and reversible changes in a bigger size range will be demonstrated. Gold nanoparticles with an original size of 15 nm will be studied. Our previous results showed that aggregation was formed through the hydrogen bonding between PAAc-10nm gold and PAAm-10nm gold. By conjugating PAAc or PAAm to 15 nm gold nanoparticles, more PAAc or PAAm can be attached to the gold surface which may result in much bigger aggregations, as compared to the 10 nm gold nanoparticles. We will also change the mixing ratio and concentration to optimize the conditions. UV-visible spectroscopy and DLS will be used to test the size of gold nanoparticles at different temperatures.
- Clotting kinetics will be measured *in vitro* with the above nanoparticles at different temperatures.

D. Studies from the Stucky lab (in collaboration with the Morrissey lab): Silica Nanoparticle (SNP) synthesis (toward Task 3, Milestone 4)

In our tests with silica nanoparticles (SNPs) and polyP-functionalized silica nanoparticles (SNP-P70), we measured the effect of the silica particles' size and concentration on coagulation. Particles above 10nm were synthesized in the laboratory following the modified Stöber method and recovered using centrifugation. The different nanoparticle sizes were obtained by varying the amounts of tetraethoxysilane (TEOS) and ammonia (NH4OH) (**Figure 14**). Sigma Aldrich supplied Ludox silica nanoparticles below 10 nm. We isolated silica nanoparticles below 50 nm by ultrafiltration and ultracentrifugation to develop a stock for coagulation and functionalization experiments. Yield posed a problem for syntheses using less than 4 % NH_4OH. Syntheses below 4 % NH4OH produced a yield below 40 % (**Figure 15**). The lack of ammonia likely prevents catalysis of the TEOS hydrolysis reaction. Zeta potential tests showed that SNPs have a negative charge in simulated body fluid, which helps activate the intrinsic pathway by activating FXII. However, zeta potential exhibits no systematic change in coagulation with respect to size or pH.

Figure 14: Particle size of SNP based on %NH4OH added.

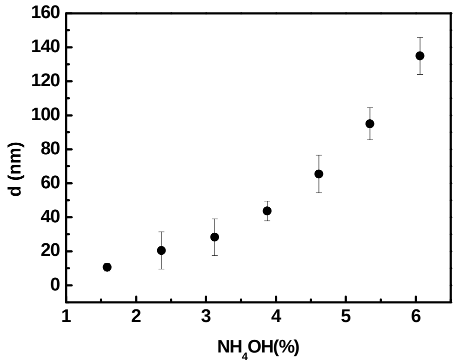

Figure 15: Silica yield based on % NH_4OH added.

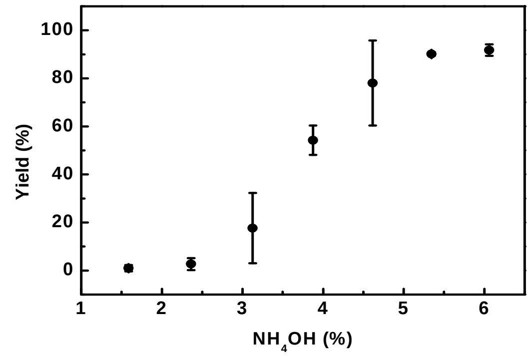

Previous clotting experiments compared the silica particles at either a fixed concentration of 0.68 mg/mL (25 mg/mL stock solution) or at a fixed size of 55 nm to determine high activity range boundaries. Each particle formed an initial clot (R) between 3 and 5 min. The current threshold for minimum R value occurs at a particle size of ~30 nm, in agreement with Margolis' earlier studies on silica coagulation. Experiments in which particles below 20 nm were synthesized exhibited a bimodal size distribution when measured using DLS. As with low yields, we attribute the bimodal size flaw to a lack of ammonia. Further experiments will use a minimum of 3% ammonia to produce sizeable yields of small nanoparticles for future clotting assays.

Figure 16. TEM micrographs of SNP of ~ 55 nm size.

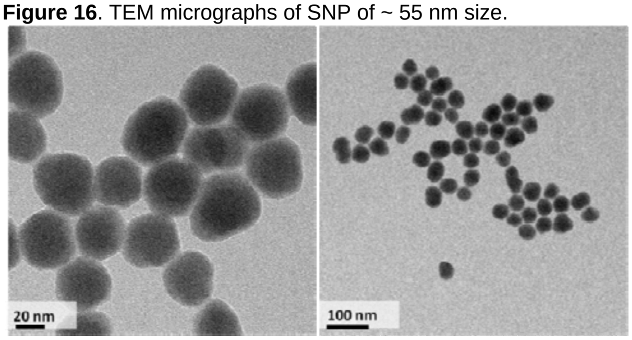

Figure 17. SNP-P70 has a shorter clotting time (R, min) at half the concentration than bare silica.Experimental conditions: 37 ºC, 11 mM Ca^{2+}.

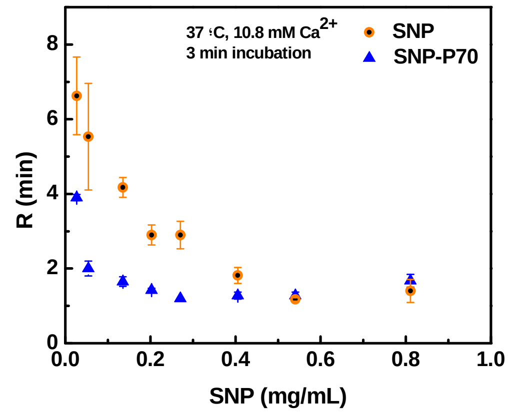

In the latest quarter, we modified our TEG protocol to mimic the Morrissey group's coagulation protocols. Utilizing phospholipids which increase coagulation through FXa, we were able to minimize R below two minutes. In **Figure 17**, the concentration dependence of R for two SNP and SNP-P70 was examined. P70 is a polyP chain that is approximately 70mer in length. It is used because P70 is roughly the same size as polyP naturally produced by activated platelets as part of the coagulation cascade. At low particle concentrations, the R value is high (clotting time is long). As the particle concentration increases, R decreases until the threshold condition is met. For bare silica, the threshold concentration occurred at 0.54 mg/ml. SNP-P70 reached a threshold at a concentration of 0.27 mg/ml, half that of bare SNP. Above the threshold concentration the R value remains low, until at much high concentration the particles may inhibit clotting due to particle aggregation or dilution of plasma factors over the particle's surface area.

Apart from the clotting time (R) other parameters are also being evaluated, such as rate of clot formation, and clot size, since the agents attached to the particle might not affect the initial clot formation time, but could accelerate the clotting when this is initiated or result in the formation of a

bigger clot. Tests confirmed that the particles maintain stability and size, at all concentrations of interest, indicating particle sizes vary solely due to synthesis conditions.

In addition to solid non-porous nanoparticles, large-pore mesoporous nanospheres (MSN) may prove valuable in delivering procoagulant proteins such as thrombin, prothombin or tissue factor to wounds. The large pore size and increased accessible surface likely increases coagulation by allowing proteins to adsorb to the surface and activate. We seek to synthesize ordered mesoporous nanoparticles in the 50-200 nm range size with a pore size between 10-30 nm. Cytotoxicity studies on mesocellular foam silica particles (MCF) show that MCF is safer for use in the body compared to the current acceptable materials such as kaolin. MCF particles with tailored coatings should be capable of circulating in the bloodstream while delivering triggering agents to the wound site.

After synthesizing the core nanoparticles, solid silica spheres, the next step becomes functionalizing the nanoparticles with a triggering agent designed to accelerate clotting. The silica scaffolds currently in use inherently initiate clotting via surface reactions with blood factors (e.g. FXII). Functionalizing the nanoparticles with polyP or prothrombin will further enhance the procoagulant nature of the particles. We have recently shown how polyP readily attaches to the surface of inorganic nanoparticles to create a more potent agent.

The polyP used in our assays was a ~70-mer length (P70) that was prepared by the Morrissey group and chosen for its similarity to the size of polyP secreted by human platelets during clotting, and which are found to activate FV. P70 directly adsorbed to silica was found to only slightly increase the particle size (by several nm). The Morrissey lab has tested SNPs generated in the Stucky lab with and without adsorbed polyP and found that P70-bound SNPs significantly decrease clotting time when compared to bare SNP (**Figure 17**). SNP-P70 also improves clotting time when compared to P70 added directly to plasma. The SNP scaffold thus serves as the best mechanism to deliver the P70 triggering agent to the wound to initiate clotting. We are exploring ways to conjugate wound-targeting peptides, for threshold switching at the local site via accumulation. We are also exploring masking the polyP with protease-cleavable appendages of PEG or cationic peptide 'neutralizers'.

Figure 18: FXa (found in the wound site) recognizes peptide sequence (IEGR) and cleaves PEG off the TSP to selectively activate coagulation.

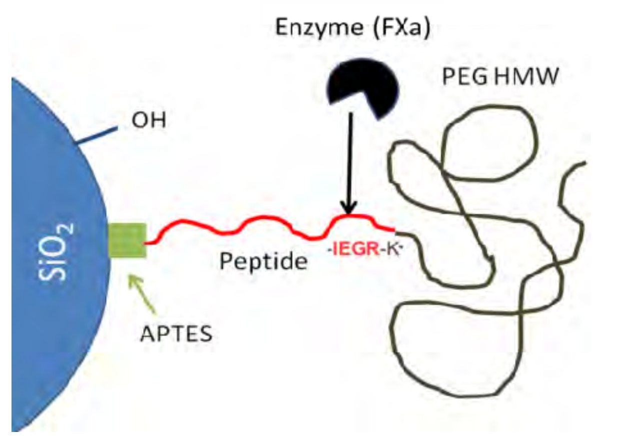

Conjugation Discussion. In comparison to external hemorrhage, the lack of tissue damage greatly impairs treatment. The particles are designed to be injected into the bloodstream and to only target bleeding sites. Thus, the particles require a second functionalization designed to protect the nanoparticles from initiating clotting in healthy vessels and inducing a heart attack or stroke. Nanoparticles designed for drug delivery often coat their particles with polyethylene glycol (PEG) to prevent unwanted activation. PEGylated nanoparticles increase the half-life of silica in the blood stream, limit cellular uptake, and limit protein adsorption to the underlying active surface. At the wound, the particle releases the PEG, revealing the active surface with which clotting is amplified. Our current studies for activation use a peptide with an IEGR sequence that connects the particle to the PEG (**Figure 18**). Activated Factor X (FXa) cleaves the peptide at the IEGR sequence, removing the PEG and leaving the activated TSP. As FXa only exists above threshold at bleeding sites, the targeting mechanism will ensure that the "swarm" of TSP activates clotting only where necessary.

In a reverse orientation where a second (targeting) peptide is on the outer tip of the PEG, we may target the damaged vascular surface, activated cell surfaces, or formation of fibrin, for example, to concentrate the pro-therapeutic at the wound site. The underlying surface will remain bare silica for initial screens and co-adsorbed polyP layers. As we advance our conjugation experience we will explore carriage of pro-proteins such as prothrombin, in comparison to direct activators of clotting by thrombin and tissue factor, each similarly masked by protease-cleavable PEG. We will use

commercially available purified proteins and determine if they can be carried in and by nanoparticles, if they can be masked by PEG, and more importantly, if they affect R values in plasma coagulation tests.

When bound to the nanoparticle surface, cross-linkers such as 3-aminopropyl triethoxysilane (APTES) limit the active surface for coagulation (**Figures 19 and 20**). We decreased the ratio of APTES to silica to obtain a PEG-linker-APTES-silica TSP that would retain a dual nature – inert in healthy blood vessels while converting to procoagulant when activated by a linker-specific protease. When functionalized solely with APTES, at low coverage, the TSP retains its procoagulant nature. When PEG attaches to these TSP via the APTES bridging elements, the TSP becomes protected. We found that coupling PEG (of at least 5kDa) decreased clotting times back to that of normal recalcified

Figure 19 - Optimization of APTES functionalization. At a ratio of 1.6 or 2.0 uL/g, SiO2-APTES is pro-coagulant while SiO2-PEG is not.

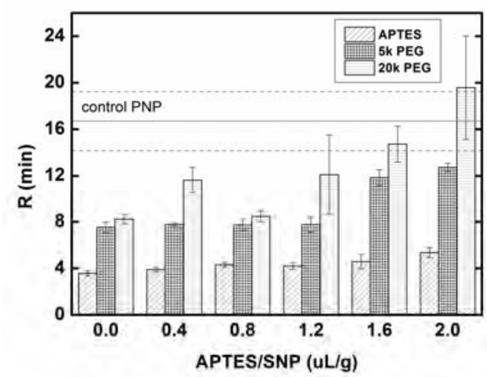

Figure 20 - Clotting times of functionalized silica particles. (Pep: peptide, PEG used is 2k).

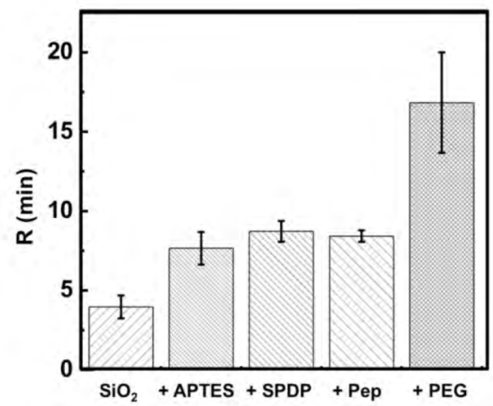

plasma. PEGylating the silica allows it to act as an anticoagulant in normal vessels. Removing PEG at the wound site activates the procoagulant activity of the TSP. We have successfully developed a candidate TSP that will activate coagulation only at a wound site.

We are continuing our efforts to refine the TSP by including a protease cleavable peptide between the APTES and PEG, to create a TSP that can remain inactivated in healthy blood vessels, while activating at a wound site. Alternative designs the TSP to expose polyP upon protease activation. In the coming months, we aim to show TSP activation by purified enzyme, which will allow us to begin testing the TSPs using microfluidic devices.

Figure 21.Clotting time (R) for various conditions using FXII deficient plasma. SiO2-P70 has the smallest and most consistent R value. Last bar is a control using pooled normal plasma.

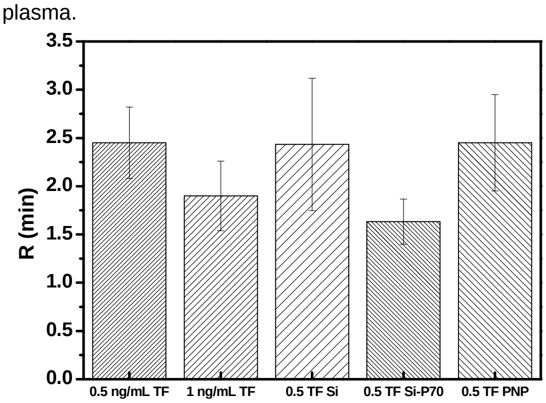

Figure 22.Coagulation Index (CI) for various conditions using FXII deficient plasma (higher index indicates increased clotting). SiO_2-P70 has the highest and most consistent CI value. Last bar is a control using pooled normal plasma.

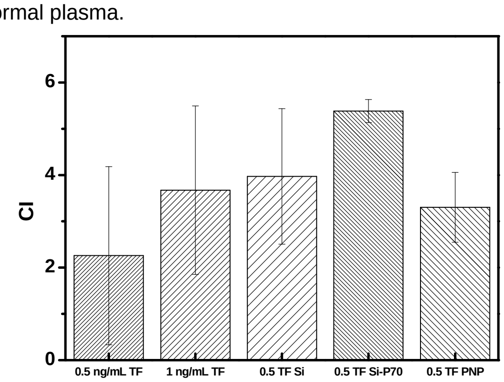

Y2 research in the Stucky lab continued on previously developed mechanisms for attaching polyP (P70) to the surface of solid silica nanoparticles. Attaching P70 through APTES will identify

possible benefits of specific functionalization of the TSP. The end goal remains attaching a procoagulant polyP chain or protein that will induce clotting solely at the desired wound site.

To further understand the mechanism by which P70-bound nanoparticles induce clotting, the Stucky group performed some clotting tests using FXII deficient plasma (Figure 21 and 22). As they activate clotting through FXII activation and the intrinsic pathway, the bare nanoparticles cannot induce clotting. With the intrinsic pathway blocked, coagulation only occurs through the addition of tissue factor (TF) and the extrinsic pathway. If P70 accelerates coagulation through FXa, a combination of TF and P70-bound silica should improve clotting. We compared various mixtures of TF and nanoparticles. In the end, the two lowest clotting times occurred as a result of either 1 ng/mL TF or 0.5 ng/mL TF mixed with 0.676 mg/mL SNP-P70. Though the two conditions shared a similar clotting time, the P70-bound silica rapidly accelerated clot growth as illustrated by the much larger coagulation index score. The P70-bound silica also exhibited the best reproducibility of all the conditions, an important characteristic to prevent adverse side-effects. The tissue factor forms a small clot rapidly upon addition to plasma, but the clot grows at a slow pace. These tests show that even under adverse conditions the P70 bound particles can quickly increase clotting through mediating FXa and thrombin. In terms of treating internal hemorrhage, this result suggests that polyP can accelerate thrombin production at an in-progress bleed to limit blood loss.

Figure 23: SNP-P70 initiates clots quicker than SNP at concentrations below 0.5 mg/ml

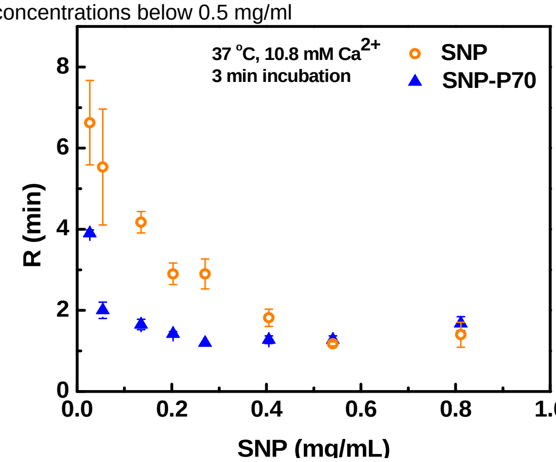

Figure 24: 1:1 SNP-P700 minimizes clot time.

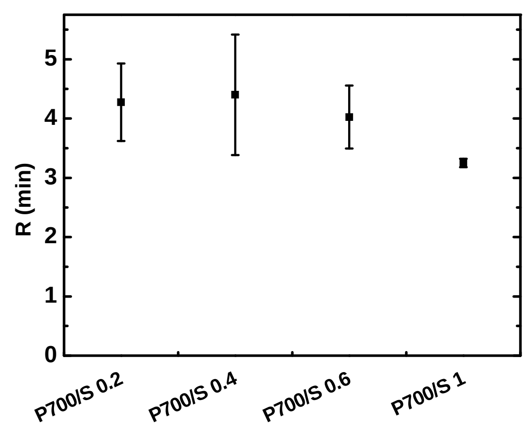

Most of Y2 research focused on quantifying the procoagulant activities of previously proposed TSPs across a range of parameters to identify important trends. Our clotting assays continued to evolve following the clotting assay protocols created by the Morrissey group. Adding a phospholipid solution and incubating the candidate TSPs in plasma prior to adding calcium showed agreement in clotting time results between the Morrissey and Stucky groups. Bare silica was tested to build a table of clotting values based on size and concentration. The same tests were repeated with P70-bound silica nanoparticles to identify potential thresholds that induced coagulation. These tests show that SNP-P70 clots plasma quicker than silica, when each are at low concentrations (**Figure 23 and 24**). The short clotting times of P70-bound silica will become more important as we move toward targeting an internal wound. Since we aim to treat internal hemorrhage throughout the body with a biocompatible TSP design to minimize potential side effects, the lower threshold of the SNP-P70 TSP will be advantageous for small concentration delivery to the body, thereby limiting potential deleterious effects.

While most of the research has focused on the shorter chain P70 polymer because of its similarity to natural polyP, we also explored longer polyPs chains. The Morrissey lab continues to develop large-scale preparations of size-fractionated polyPs. The first shipment consisted of ~700-mer polyP (P700). PolyP with a size range above 500mers is shown to accelerate the contact or intrinsic pathway by activating FXII. The P700 was attached to the scaffolds using the same methods. Four different ratios of P700:SNP were tested – 0.2, 0.4, 0.6, and 1. Similarly to P70, preliminary

clotting assays suggest that clot time decreases with a ratio of P700:SNP above 0.5. Currently, a 1:1 ratio minimizes clot time (Figure 10). We hope to verify this data in the coming year. Finally, we seek to identify apparent rate differences between P70 and P700 using FXII deficient plasma to inhibit the intrinsic pathway.

In keeping with the goal of treating internal hemorrhage, we will focus on applying particles in concentrations well below the threshold level to prevent nonspecific clotting during general circulation. Spatially targeting the materials to the specific surfaces (i.e. wounded endothelial) or via other unique factors would then concentrate the material to above-threshold clotting behavior, though this is not required for our near-future steps. Protecting the particles with PEG, which is cleaved off by factors present at the target site, would add an additional level of control.

In addition to testing the particles in the Stucky lab, 200-mg samples of SNP, SNP-P70, and SNP-P700 nanoparticles were sent to the Morrissey lab for polyP quantification and further coagulation tests. These tests revealed that SNP-P70 particles with a concentration of roughly 25 nmol PO_4/ mg SNP (quantified by hydrolysis) exhibited higher procoagulant activity than SNP-P70 particles with a higher nmol PO4/ mg SNP concentration. Morrissey group, please add a summary paragraph.

In addition to TEG, we also tested the coagulation threshold response using a thrombin-specific blue coumarin dye. Our experiments use the method established by the Ismagilov group in prior clotting threshold studies. A small concentration of dye is added to the recalcified plasma. As clotting progresses and thrombin is produced, the thrombin cleaves the coumarin dye causing the solution to fluoresce. Signified by rapid fluorescence, the thrombin burst quickly leads to clot formation. A fluorescence microscope captures the qualitative change as shown in **Figure 25**.

Figure 25 - (A) Blue coumarin dye experiment at time 0 min. (B) Blue coumarin experiment at time 20 min.

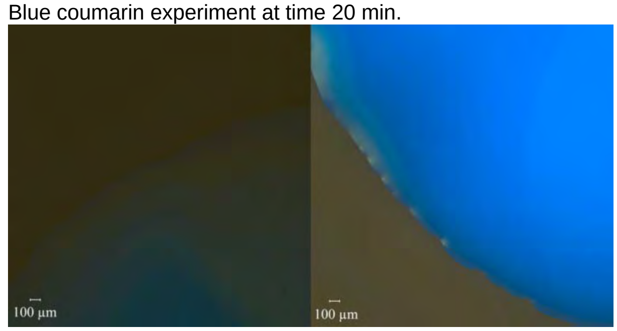

Due to the microscope's limitations in quantifying thrombin expression, we instead monitored thrombin generation using a plate reader. By reading fluorescence every 10 seconds, we can clearly identify the thrombin burst. As clotting occurs near the rapid rise section of the thrombin burst, we can determine the clot time from the fluorescence data plot.

After determining the procoagulant activity of SNP-P70 under normal conditions, we sought to apply the SNP-P70 TSPs under traumatic conditions. A traumatic injury can quickly develop into coagulopathy, the fundamental breakdown of the human coagulation cascade. Though coagulopathy can exist either as a hypercoagulant or hypocoagulant form, we will define coagulopathy as the fundamental breakdown of the coagulation cascade that impairs clot formation. In the presence of trauma, the coagulopathic body becomes so weakened that anticoagulant pathways take over and a clot cannot form. Eventually, the patient succumbs to blood loss. Roughly 25 % of trauma patients exhibit coagulopathy upon admission to hospitals.

Coagulopathy exists in three states known as the "lethal triad" - dilution, hypothermia, and acidosis. Each damages the cascade in a specific way. In a coagulopathic state, all three states combine to inhibit clot formation. Left untreated, coagulopathic injuries often prove fatal. In our experiments we mimic dilution using a phosphate buffered solution (PBS). Incubating plasma below the usual 37^{o}C creates hypothermic conditions. Finally, we use a dilute phosphoric acid solution to acidify the plasma below a pH of 7.1. The experiments utilize a set concentration of lipidated tissue factor (LTF) – 0.5 ng/ml for TEG tests, 0.185 ng/ml for fluorescence dye tests – to ensure timely initiation of the coagulation cascade through the extrinsic pathway and the body's main response to vessel injury. The SNP-P70 candidate TSP was tested at 0.25mg/ml without LTF to compare its ability to form clots.

As blood flows out of the body, the concentrations of proteins and factors in the blood flow out as well. Due to the loss of both procoagulant and anticoagulant factors, dilution only begins to significantly inhibit clotting at the ~50 % level. After reaching the 50 % threshold, the loss of procoagulant materials apparently is too much for the cascade to bear. Using TEG and dye fluorescence, we established a dilution baseline. We then attempted to reverse the coagulopathic conditions using SNP-P70 at the threshold concentration of ~ 0.25mg/ml identified in our TEG experiments. SNP-P70 successfully hastens thrombin burst and clot formation. However, SNP-P70 cannot improve the final clot size, which remains smaller than normal (**Figure 26 and 27**). The severe dilution of fibrinogen causes the small clot size. Without fibrinogen, the physical clot cannot form. In light of this data, we can consider delivering fibrinogen in addition to SNP-P70 to treat trauma patients suffering from massive bleeding and hemodilution.

Figure 26 - SNP-P70 generates thrombin quicker than SNP.

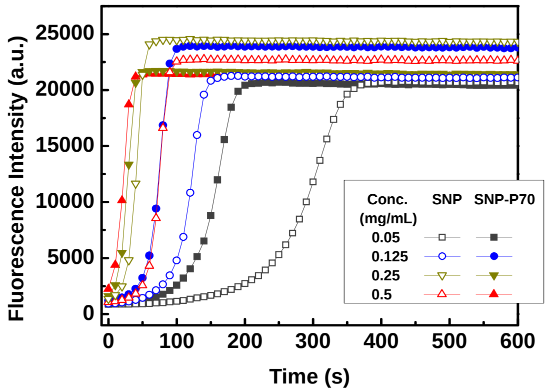

Figure 27 - he same fluorescence data presented in terms of clot time.

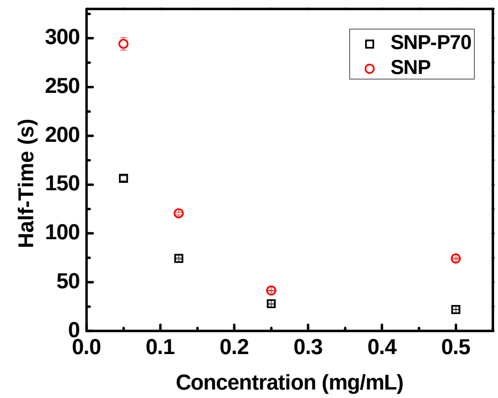

Hypothermia, the second member of the lethal triad, occurs when the body temperature drops below 37°C. The drop in temperature leads to a decreased rate in the kinetics of many of the coagulation factors, especially formation of the tissue factor – FVIIa (TF-FVIIa) complex during the initiation phase of coagulation. Unlike dilution where fibrinogen deficit triggers the drop in clotting, hypothermia slows coagulation but does not prevent it. The addition of SNP-P70 to hypothermic plasma results in improved coagulation across all TEG parameters. To highlight the excellence of SNP-P70 in clotting at sub-normal body temperature, we use the coagulation index formula to show robust procoagulant nature of the candidate TSP. Coagulation index (CI) combines all four TEG facets – R, K, alpha, and MA – into a single value; the more positive the CI, the stronger the

Figure 28A - Thrombin generation times from 100 % plasma to 25 % plasma; i.e.: 100 % is 100 % plasma and 0 % dilutant.

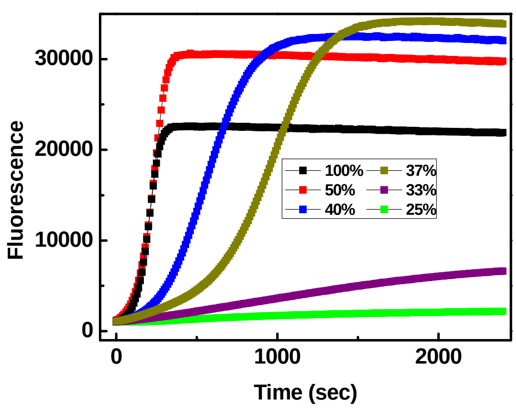

Figure 28B - Adding SNP-P70 generates thrombin quickly even under severe plasma dilution.

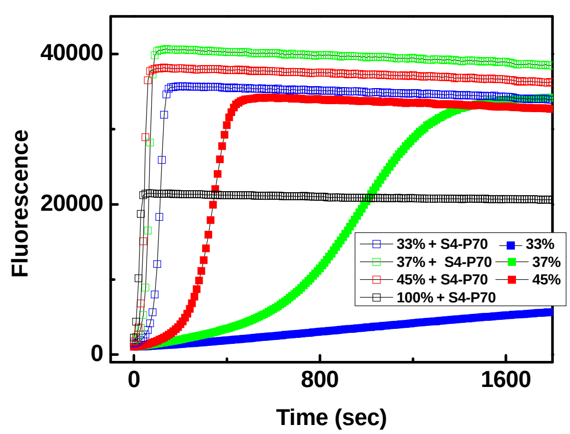

procoagulant. While promising, our experiments on both the TEG and plate reader have showed some unexpected anomalies at 32°C and below (**Figure 29**). We will continue to work on the hypothermic states in Y3 to ensure that the data is reliable.

Figure 29A - SNP-P70 TSPs initiate clots quicker under hypothermia.

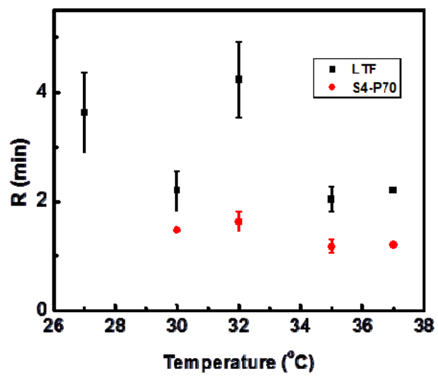

Figure 29B - SNP-P70 improves clot formation immensely compared to LTF.

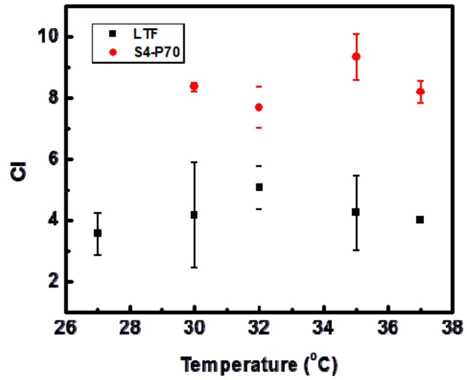

Of the triad, acidosis causes the greatest problem to trauma patients. Normal blood has a pH of 7.4, which drops as a result of trauma. While sodium bicarbonate can return the blood's pH to a normal level, effects from acidosis continue to plague coagulopathic patients for roughly 24 hours. We will test the response of acidotic plasma to SNP-P70 in Y3. Our goal is to show SNP-P70 can correct deficiencies in clotting for all triad conditions, dilution, hypothermia, and acidosis.

In Y2, the research focus has shifted from designing and creating candidate TSPs to quantifying the procoagulant activities of TSPs. Our research has shown that SNP-P70 outperforms bare SNP and LTF in lowering clot times while forming strong clots. As discovered by the Morrissey group, studies on FXII deficient plasma show that SNP-P70 initiates clotting through FXa coagulation pathway. Finally, SNP-P70 has been shown to decrease clot time and quicken thrombin generation under coagulopathic conditions often found in patients who have suffered a traumatic wound. In static conditions, SNP-P70 appears an excellent candidate for treating internal hemorrhage. In the coming year, we aim to test targeting strategies under flow conditions to test the viability of SNP-P70 in treating internal hemorrhage.

KEY RESEARCH ACCOMPLISHMENTS

Production of raw materials for conjugation to nanoparticles:

- Developed reproducible and scalable procedures for production of gram quantities of purified polyP of carefully defined size ranges, which is important in controlling the procoagulant activity of polyP

Development of polyP-conjugated gold nanoparticles:

- Synthesized gold nanoparticles with controlled particle size distributions
- Synthesized polyP-gold nanoparticle conjugates (with various sizes and ratios of polyP to gold nanoparticles) to verify the threshold conditions of blood coagulation
- Developed a thermo-sensitive system of PAAc- and PAAm-gold nanoparticle conjugates, which may potentially possess controllable and reversible aggregation due to temperature changes in human bodies

Development of polyP-conjugated silica nanoparticles (SNP):

- Determined that ~ 55 nm size SNP are the ideal scaffold for supporting particles due to minimal clot time and maximum synthesis yield
- Developed new particle synthesis procedure for delivery of thrombin, which has a hydrodynamic radius of 8.4 nm
- Refined procedure for attaching medium length (70mer = P70) and long chain (500-1500mer) polyP to silica nanoparticles using Lewis acid-base chemistry to create candidate particles
- Developed APTES bridge for attaching PEG to SNPs to create a switchable particle that is anticoagulant in healthy blood vessels and procoagulant at wound site
- Optimized APTES-SNP for PEG-switchable concentration-dependence of particles
- Developed large quantity synthesis for polyP-bound nanoparticles
- Identified a threshold concentration of SNP-P70 at ~ 0.25 mg/ml to minimize clot time and thrombin generation time
- Identified a threshold concentration of bare SNP at ~ 0.5 mg/ml to minimize clot time and thrombin generation time
- At ~0.25mg/ml threshold, SNP-P70 successfully lower clot time and thrombin generation time under severe dilutional coagulopathic conditions
- At ~0.25mg/ml threshold, SNP-P70 successfully lower clot time, lower thrombin generation time, and improve overall clot formation under hypothermic coagulopathic conditions
- Established limited human cell cytotoxicity and overall biocompatibility of porous silica

REPORTABLE OUTCOMES

- The Ismagilov lab received approval from the Office of Research Protections to obtain human blood samples
- Manuscripts in Preparation (for submission in the near future)
- Controlled and Reversible Aggregation of Gold Nanoparticles
- Threshold Conditions for PolyP-Gold Nanoparticles Conjugates to Trigger Blood Coagulation through Contact Pathways

Recent Publications:

- Li, Y., Sawvel, A. M., Jun, Y.-S., Nownes, S., Ni, M., Kudela, D., Stucky, G. D., Zink, D. Cytotoxicity and potency of mesocellular foam-26 in comparison to layered clays used as hemostatic agents. Toxicology Research, in press.

Recent Presentations:

- Stucky GD, "Molecular assembly of material systems with integrated nanoscale to macroscale functionalities," The 2nd International Symposium on Advanced Composite Materials, Tokyo, Japan, November 7-8, 2011.
- Stucky GD, "Zeolites and R. M. Barrer Inspired Control of Bioprocesses: The Challenge of Hemostasis," The Pennsylvania State University Barrer Lecture, University Park, PA, April 14, 2011.
- Stucky GD, "Controlling Bioprocesses with Inorganic Nanostructured Systems:
- The Challenge of Hemostasis," University of California, Berkeley Student-Hosted Inorganic Chemistry Series, Berkeley, CA, February 25, 2011.
- Morrissey, JH. "Modulation of Hemostasis, Thrombosis, and Inflammation by PolyP "Special Symposium on the Basic Science of Hemostasis and Thrombosis, Annual Meeting of the American Society of Hematology, Atlanta, GA, December 11, 2012.

CONCLUSION

Specific Aim #1 of the statement of work calls for using theory and experiments to identify the most promising mechanisms to switch from below- to above-threshold conditions to initiate local clotting. The Ismagilov lab has been delayed in pursuing this aim owing to its relocation to Caltech. Now that the Ismagilov lab has been successfully relocated and the necessary subcontracts and other regulatory approval have been secured, these simulation experiments will proceed in the next grant period.

Specific Aim #2 of the statement of work calls for the design of a threshold-switchable particle system with a paired particle and trigger to target internal hemorrhage. The proposal calls for us to identify nanoparticles as scaffolds and to test procedures for attaching procoagulant materials to the nanoparticles. The Morrissey lab has developed high-yield, scalable methods for carefully size-fractionating polyP so that sufficient quantities can now be utilized in producing nanoparticles by the Stucky and Liu labs. The Stucky group's contributions have focused most substantially on silica nanoparticles as viable scaffolds to treat internal hemorrhage, while the Liu group has focused on most substantially on gold nanoparticles as scaffolds. In coordination with the Morrissey group, research has focused quantifying the parameters that modulate the procoagulant activities of the various candidate nanoparticles formulations. Going forward, work with the Ismagilov group will focus on determining the threshold conditions for these nanoparticles.

In the coming year, the Ismagilov group will use numerical simulations to refine the parameters for TSP-induced blood clotting and identify threshold conditions. Now that they have approval for drawing blood from human volunteers, they will proceed with setting up and performing microfluidic tests of the properties of candidate particles using freshly isolated human blood. The Liu group will continue to develop and mature gold-based polyP-nanoparticles and refine their clotting characteristics in collaboration with the Morrissey lab. The Stucky group will continue to refine the syntheses and capping procedures to provide large quantities potential TSPs to the Ismagilov and Morrissey groups for threshold testing. The goal remains to identify several new TSP systems with the potential to treat internal hemorrhage.

"So-What Section": The final goal of these studies is to develop advanced nanoparticles engineered to stop internal (incompressible) hemorrhage. If we are successful, we will create regulated clotting activators that can circulate in the blood at below the threshold necessary to trigger clotting, and therefore not cause unwanted thrombosis. However, the nanoparticles will ultimately be engineered to accumulate at sites of internal injury/bleeding, where their local concentration will greatly exceed the threshold for clotting activation, thereby restoring hemostasis. This has the potential to treat otherwise untreatable, life-threatening internal bleeding associated with trauma.

REFERENCES

[1] Smith SA, Mutch NJ, Baskar D, Rohloff P, Docampo R, Morrissey JH. Polyphosphate modulates blood coagulation and fibrinolysis. Proc Natl Acad Sci U S A. 2006;103:903-8.

[2] Morrissey JH, Choi SH, Smith SA. Polyphosphate: an ancient molecule that links platelets, coagulation, and inflammation. Blood. 2012;119:5972-9.

[3] Muller F, Mutch NJ, Schenk WA, Smith SA, Esterl L, Spronk HM, et al. Platelet Polyphosphates Are Proinflammatory and Procoagulant Mediators In Vivo. Cell. 2009;139:1143-56.

[4] Shoffstall AJ, Atkins KT, Groynom RE, Varley ME, Everhart LM, Lashof-Sullivan MM, et al. Intravenous hemostatic nanoparticles increase survival following blunt trauma injury. Biomacromolecules. 2012;13:3850-7.

[5] Kimling J, Maier M, Okenve B, Kotaidis V, Ballot H, Plech A. Turkevich method for gold nanoparticle synthesis revisited. Journal of Physical Chemistry B. 2006;110:15700-7.

[6] Choi SH, Collins JNR, Smith SA, Davis-Harrison RL, Rienstra CM, Morrissey JH. Phosphoramidate End Labeling of Inorganic Polyphosphates: Facile Manipulation of Polyphosphate for Investigating and Modulating Its Biological Activities. Biochemistry. 2010;49:9935-41.

[7] Mucha A, Grembecka J, Cierpicki T, Kafarski P. Hydrolysis of the phosphonamidate bond in phosphono dipeptide analogues - The influence of the nature of the N-terminal functional group. European Journal of Organic Chemistry. 2003:4797-803.

[8] Mucha A, Kunert A, Grembecka J, Pawelczak M, Kafarski P. A phosphonamidate containing aromatic N-terminal amino group as inhibitor of leucine aminopeptidase - design, synthesis and stability. European Journal of Medicinal Chemistry. 2006;41:768-72.

[9] Jacobsen NE, Bartlett PA. A Phosphonamidate dipeptide analog as an inhibitor of carboxypeptidase-a. Journal of the American Chemical Society. 1981;103:654-7.

[10] Garrison AW, Boozer CE. The acid-catalyzed hydrolysis of a series of phosphoramidates. Journal of the American Chemical Society. 1968;80:3486-94.

[11] Haake P, Ossip PS. Phosphinylium ions as intermediates in solvolysis of sterically hindered phosphinyl chlorides Tetrahedron Letters. 1970:4841-&.

[12] Demers LM, Mirkin CA, Mucic RC, Reynolds RA, Letsinger RL, Elghanian R, et al. A fluorescence-based method for determining the surface coverage and hybridization efficiency of thiol-capped oligonucleotides bound to gold thin films and nanoparticles. Analytical Chemistry. 2000;72:5535-41.

[13] Rickwood D. Centrifugation: A Practical Approach. 2 ed. Oxford, U.K., Washington, D.C.: IRL press; 1984.

[14] Roca M, Pandya NH, Nath S, Haes AJ. Linear Assembly of Gold Nanoparticle Clusters via Centrifugation. Langmuir. 2010;26:2035-41.

[15] Wilson K, Walker J. Principles and Techniques of Biochemistry and Molecular Biotechnology. 7 ed. New York: Cambridge University Press; 2010.

[16] Kastrup CJ, Boedicker JQ, Pomerantsev AP, Moayeri M, Bian Y, Pompano RR, et al. Spatial localization of bacteria controls coagulation of human blood by 'quorum acting'. Nature Chemical Biology. 2008;4:742-50.

[17] Fahim M. Effect of hypoxic breathing on cutaneous temperature recovery in man. International Journal of Biometeorology. 1992;36:5-9.

[18] Wang Q, Li S, Wang Z, Liu H, Li C. Preparation and Characterization of a Positive Thermoresponsive Hydrogel for Drug Loading and Release. Journal of Applied Polymer Science. 2009;111:1417-25.

[19] Basu S, Ghosh SK, Kundu S, Panigrahi S, Praharaj S, Pande S, et al. Biomolecule induced nanoparticle aggregation: Effect of particle size on interparticle coupling. J Colloid Interface Sci. 2007;313:724-34.

[20] Levy R, Thanh NTK, Doty RC, Hussain I, Nichols RJ, Schiffrin DJ, et al. Rational and combinatorial design of peptide capping Ligands for gold nanoparticles. Journal of the American Chemical Society. 2004;126:10076-84.

[21] Smith RM, Hansen DE. The pH-rate profile for the hydrolysis of a peptide bond. Journal of the American Chemical Society. 1998;120:8910-3.